Hyperoxia Induced Chromatin Remodeling in Mesenchymal Stromal Cells

Lauren A. Monroe[1, 3], Samantha Kaonis[1, 3], Neda Kabi[1, 3], Soham Ghosh[1, 2, 3, 4 *]

[1]School of Biomedical Engineering, Colorado State University, Fort Collins, CO

[2]Department of Mechanical Engineering, Colorado State University, Fort Collins, CO

[3]Translational Medicine Institute, Colorado State University, Fort Collins, CO

[4]Cell and Molecular Biology, Colorado State University, Fort Collins, CO

*Corresponding author: Soham Ghosh, Email: soham.ghosh@colostate.edu

ABSTRACT

Chromatin is a highly dynamic entity of the eukaryotic cell nucleus. New evidences are emerging with a support of the notion that chromatin can locally and globally rearrange itself to adapt with the cellular microenvironmental changes. Such changes include oxidative stress such as supraphysiological oxygen level, found in hyperoxia. Although it is known that hyperoxia can cause DNA damage and alterations in cell function, it is not well understood how the chromatin architecture changes under such condition and what is the functional significance of such change. Characterization and quantification of chromatin remodeling is therefore a first step to understand the chromatin dynamics for understanding complex subnuclear behavior under single or multiple environmental stresses. Towards that end, in this work, human bone marrow derived mesenchymal stromal cells were used to characterize such chromatin level alterations under the changing oxidative stress on cells. Hyperoxia was applied using hydrogen peroxide treatment. Chromatin remodeling was hindered by the inhibition of methyltransferase EZH2, which regulates ARID1A activity and chromatin compaction. Epigenetic modifications and DNA damage under hyperoxia was investigated, which was found affected by the pharmacological inhibition of chromatin remodeling. The developed techniques and findings might provide us with new mechanism and intervention strategies to target genotoxic hyper-oxidative stress, which is common in degenerative diseases and aging, and also for cell therapy in regenerative medicine.

KEYWORD

Chromatin Remodeling, Hyperoxia, Epigenetics, Mesenchymal Stromal Cell, Histone Modification

INTRODUCTION

Cells are known to accumulate DNA damage during their lifetime through natural processes such as cellular metabolism where reactive oxygen species (ROS) is a natural by-product. As an organism ages, ROS can accumulate leading to more DNA damage. Additionally, environmental stresses that are common in physiological systems can also generate ROS. The hyper oxidative condition or hyperoxia is caused by the generation and accumulation of ROS. Hyperoxia damages cellular macromolecules, including DNA, resulting in cell apoptosis and senescence (1). With aging and tissue degeneration, the hyper-oxidative stress increases (2, 3). Concomitantly, antioxidants may stimulate cell survival.

Cells demonstrate a variety of responses towards the environmental stress. Such environmental stress in common in culture conditions *in vitro* and also *in vivo* (4). A common downstream effect of such environmental stresses including the hyper-oxidative stress is DNA damage (5–7). In epithelial and other cells, the chromatin is shown to remodel for protecting the nucleus from the adverse effects of the DNA damage lesion (8–11). DNA damage is known to soften the chromatin architecture to either create a protective dense heterochromatin barrier to stop the damage response spreading into the nucleus, or the damaged DNA lesion may be carried to an open euchromatin region for efficient damage correction (11, 12). However, it is not understood what the steps post exposure to hyper-oxidative stress are which facilitate such chromatin remodeling.

Oxidative stress is particularly critical for stem cells such as mesenchymal stem/ stromal cells (MSC). MSCs are activated *in vivo* under physiological stress. From multiple lines of evidence, it was suggested that MSCs are deployed for regeneration (5, 13) when the tissue they are residing in is physiologically stressed, as seen in degenerative conditions associated with aging and diseases such as osteoarthritis and bone injury. Stress inducing condition has been exploited to mobilize and activate MSC for enhanced regeneration *in vivo* (14–16). Since no technology currently exists to directly investigate the stress response or to even visualize individual MSC *in vivo* (17, 18), the stress response has been investigated using a reductionist *in vitro* (5) approach. Stress inducing physiological conditions include oxidative condition, mechanical stretch and metabolic stress. Under these conditions, MSC show higher activation, differentiation and proliferation (19–27). However, under prolonged stress events, the MSC become 'aged' or senescent. Maintenance of optimal oxidative status is critical

for tissues and for MSC to survive and regenerate during its lifetime (28–31). Additionally, for regenerative medicine applications MSC are expanded and injected inside the body where they are exposed to high amount of oxygen toxicity (32, 33), associated with inflammatory conditions.

Although it is clear that MSC undergo damages *in vitro* and *in vivo* under physiological stresses including oxidative stress, it is not clear what happens inside the MSC or any other cells at the chromatin level after the exposure to hyper-oxidative stress due to technical limitations to investigate such events. In this study, we aim to discover these underlying mechanisms using advanced microscopy and image analysis techniques. Understanding such mechanism might provide us with new mechanism and intervention strategies to target genotoxic stress, which is common in degenerative diseases and aging, and also for cell therapy in regenerative medicine.

The dynamic nature of the intranuclear space within cells plays a crucial role in gene expression regulation over time, with chromatin remodeling emerging as a key mechanism. This remodeling is facilitated through various epigenetic processes, such as Chromatin Remodeling Complex (CRC) (17-21) and histone modifications, which locally condense or decondense chromatin. Although the detailed mechanism and functional significance of chromatin remodeling have recently come to light, a specific type of remodeling occurs at the multi-nucleosome level, where ATP-dependent chromatin remodelers play a critical role. The intricate details of chromatin remodeling, involving processes like nucleosome sliding, engagement, and ejection, are still being uncovered. However, various classes of CRC, including SWI/SNF (SWItch/ Sucrose Non-Fermentable), have been identified. The core protein in the SWI/SNF complex, ARID1A, maintains a delicate balance with EZH2. ARID1A, as part of SWI/SNF, governs chromatin remodeling, suggesting that inhibiting EZH2 could potentially disrupt the chromatin remodeling process (34). Consequently, intervening pharmacologically with EZH2 offers an opportunity to explore the role of chromatin remodeling in cellular functions, especially during sudden perturbations that may necessitate chromatin remodeling.

In this study we hypothesized that chromatin remodeling occurs through the engagement of ARID1A function during the MSC exposure to hyper-oxidative stress. To test this hypothesis, we visualized and characterized the chromatin remodeling at high spatiotemporal resolution in MSC undergoing hyper-oxidative stress by hydrogen peroxide using a newly developed imaging assay. Chromatin remodeling was impeded by the

inhibition of methyltransferase EZH2, which regulates ARID1A activity and chromatin compaction with a drug GSK126. After thorough characterization of how GSK126 affects the MSC phenotype and several epigenetic modifiers, the effect of GSK126 on chromatin remodeling under hyperoxia was investigated. Finally, DNA damage was visualized in nuclei under hyper-oxidative stress and by the inhibition of chromatin remodeling using GSK126. The results are discussed to provide novel insights into the role of chromatin remodeling during oxygen toxicity, with possible implications in cellular physiology in health, disease and regenerative medicine.

MATERIALS AND METHODS

Cell culture and pharmacological treatment

Human bone marrow derived primary MSC (hBM-MSC) were used for this study. Cells from healthy adults were obtained from Lonza at passage 2 (PT-2501). Cells were subcultured using Lonza MSC general medium (MSCGM) consisting of MSC basal medium and growth supplements (MCGS) and maintained at 37°C, 90% humidity and 5% CO_2. Trypsin EDTA (Lonza) were used for passaging. For all live experiments, cells were maintained in the MSCGM. For all imaging experiments, ibidi 8 well μ-slides (ibidi 80826) were used. They are already treated for cell culture and consists of a thin polymer coverslip at the bottom for imaging. Cells were seeded at 5000/ cm^2. Cells were exposed to the drug GSK126 at 20 μM concentration (Sigma Aldrich), one day post seeding and attachment. The control groups contained DMSO to match the concentration of the drug's dilutant which is also DMSO (VWR). After 2 days of drug treatment, cell proliferation was quantified and after 4 days of drug treatment, cells were used for hydrogen peroxide exposure study. Hydrogen peroxide was diluted in DPBS to prepare 500 μM solution in MSCGM, with or without GSK126 as required for the experiments.

Quantification of cell proliferation and cell viability

After 3 days of complete cell proliferation (1-day pre drug treatment, 2 days post GSK126 addition) cells were fixed with 4% PFA (in 1X PBS: Phosphate Buffer Solution) for 7 minutes at room temperature. DAPI (Thermo Fisher) was used to stain the nuclei. Images were captured at multiple random locations. Subsequently, the images were thresholded in ImageJ and the particle analyzer was used to count the number of cells in the fields of view. That number was used to extrapolate the cell number per well (total area per well is 1 cm^2). Then the initial cell seeding number (5000/ cm^2) was used to calculate the fold change of cell number at day 3 compared

to the initial number of seeded cells. Cell viability for all cases was performed using a live/dead assay kit (Thermo Fisher) consisting of Calcein AM and ethidium homodimer according to the manufacturer's protocol. Cells were imaged using a confocal microscope (Zeiss LSM 980) in the 488 nm (green) and 561 nm (red) channels. The required ratio of Calcein AM and ethidium homodimer was calibrated beforehand for the specific cell type.

Quantification of cell and nuclear phenotype & immunofluorescence staining

Fixed cells were stained with phalloidin and DAPI (Thermo Fisher) to quantify the cell and nuclear phenotype. Images were acquired using a Zeiss LSM 980 microscope. ImageJ was used to characterize the cell and nuclear geometric parameters such as area, perimeter, P/A, solidity and circularity as described in a previous study (35). The fluorescence intensity of the F-actin was quantified using the "plot profile" tool. For immunofluorescence studies, cells were permeabilized with 0.1% Triton X-100 in 1X PBS, washed with 1X PBS, blocked for non-specific binding sites with bovine serum albumin and normal goat serum. Primary antibody was diluted at the required concentration in antibody dilution buffer and incubated overnight at 4°C. Next, secondary antibody was applied at the required concentration at room temperature for 2 hours. Next, DAPI and phalloidin staining was performed as required. Cells were imaged using a confocal microscope (Zeiss LSM 980) using several objective lenses (10×, 20×, 40× water objective or 63× oil objective) as required for the specific experiment. Super-resolution microscopy was performed using the Airyscan 2 module of the confocal microscope and 63× oil objective. The following antibodies were used for this study. Conjugated antibodies: H3K4Me3 (CST, 9751, 1:100), H3K27Me3 (CST, 9733, 1:100); Unconjugated primary antibodies: H3K9Me3 (Invitrogen, PA5-31910, 1:400), Phospho-Histone H2A.X (Invitrogen, MA1-2022, 1:200); Secondary antibodies: Alexa Fluor highly cross-adsorbed (Invitrogen A32731, Invitrogen A32733 and Invitrogen A32727, all in the ratio 1:200).

Live imaging of chromatin remodeling

To image the live cell response to hydrogen peroxide, NucBlue was added to the ibidi plate wells (2 drops/ml) and maintained inside the incubator for 20 minutes at 37°C, 90% humidity and 5% CO_2. After that the plate was placed on the confocal microscope stage and the subsequent imaging was performed using the 40× water objective lens for high resolution imaging with the 405 nm laser. The sample was maintained at 37°C, 90% humidity and 5% CO_2 during the imaging session using an incubation chamber. After choosing a suitable nucleus,

the crop area was increased to visualize a single nucleus with detailed chromatin architecture. Once the nucleus was decided, an image was captured before adding the hydrogen peroxide. At this stage, the medium was pipetted out and medium containing H_2O_2 was added (with or without GSK126). Immediately after that step, the nucleus was imaged again. Images were then captured every 5 minutes for 80 minutes.

Quantification of chromatin remodeling

After the live imaging was performed, the images were cropped and prepared for further postprocessing using ImageJ. A custom Matlab code was developed for quantification of the chromatin remodeling index (CRI). The CRI was calculated at every timepoint with respect to the image corresponding to the pre-H_2O_2 treatment. The images were registered using a series of in-house Matlab function instructions. This step registered each pixel of the pre-H_2O_2 treatment image with the pixels of the post-H_2O_2 treatment timepoints. The result was a set of coordinates (X_t, Y_t) at every post-H_2O_2 treatment timepoint and initial coordinate (X_i, Y_i) of the pre-H_2O_2 treatment. Accordingly, the CRI was calculated by using the following equation: $CRI = [(X_t - X_i)^2 + (Y_t - Y_i)^2]^{1/2}$ Note that this quantity is in pixels which can be converted to microns if required. Before the registration code was applied, a drift correction algorithm was implemented to the image stack using ImageJ to account for any bulk drifting of the nucleus. Therefore, the CRI only accounted for the real chromatin motion, and discarded any other movement of the bulk nucleus. This technique is limited only by the image resolution. We define the displacement map as a chromatin remodeling index map for this specific context. This technique has been thoroughly validated in previous studies (36). Segregation of chromatin domains was performed to quantify CRI in the intranuclear space. This step was performed based on a previously published work (37). The pixels of the raw image were sorted based on the grayscale pixel intensity, which can have any integer value between 0 and 255, where 0 is absolute black and 255 is absolute white. Hill function was fit to the dataset. Subsequently, a user independent automated algorithm was utilized to segregate the euchromatin, interchromatin and heterochromatin domains.

Statistics

T-tests were used to quantify differences between the groups. Error bars in bar graphs represent the standard deviation. The number of technical replicates, number of cells (when applicable), and p-values are reported in each individual figure.

RESULTS

GSK126 lowers the cell proliferation by affecting chromatin remodeling but does not affect cell phenotype

Cell proliferation assays through imaging revealed a significant reduction in MSC proliferation at 20 µM GSK126, as depicted in Figure 1A. Notably, there were no discernible visual alterations in cell or nuclear phenotype between the control and GSK126-treated groups. The proliferation rate exhibited a nearly 60% decrease over a 3-day period with GSK126 treatment, as illustrated in Figure 1B and 1C. Despite this reduction, MSCs maintained their characteristic spindle-like shape and elliptical nucleus in both experimental conditions, as quantified using conventional geometric parameters (Figure 1D, E).

GSK126 exerts its effect on chromatin remodeling by inhibiting EZH2, thereby impacting the dynamics of ARID1A, a key component of the SWI/SNF chromatin remodeler, or by influencing H3K27 methylation,

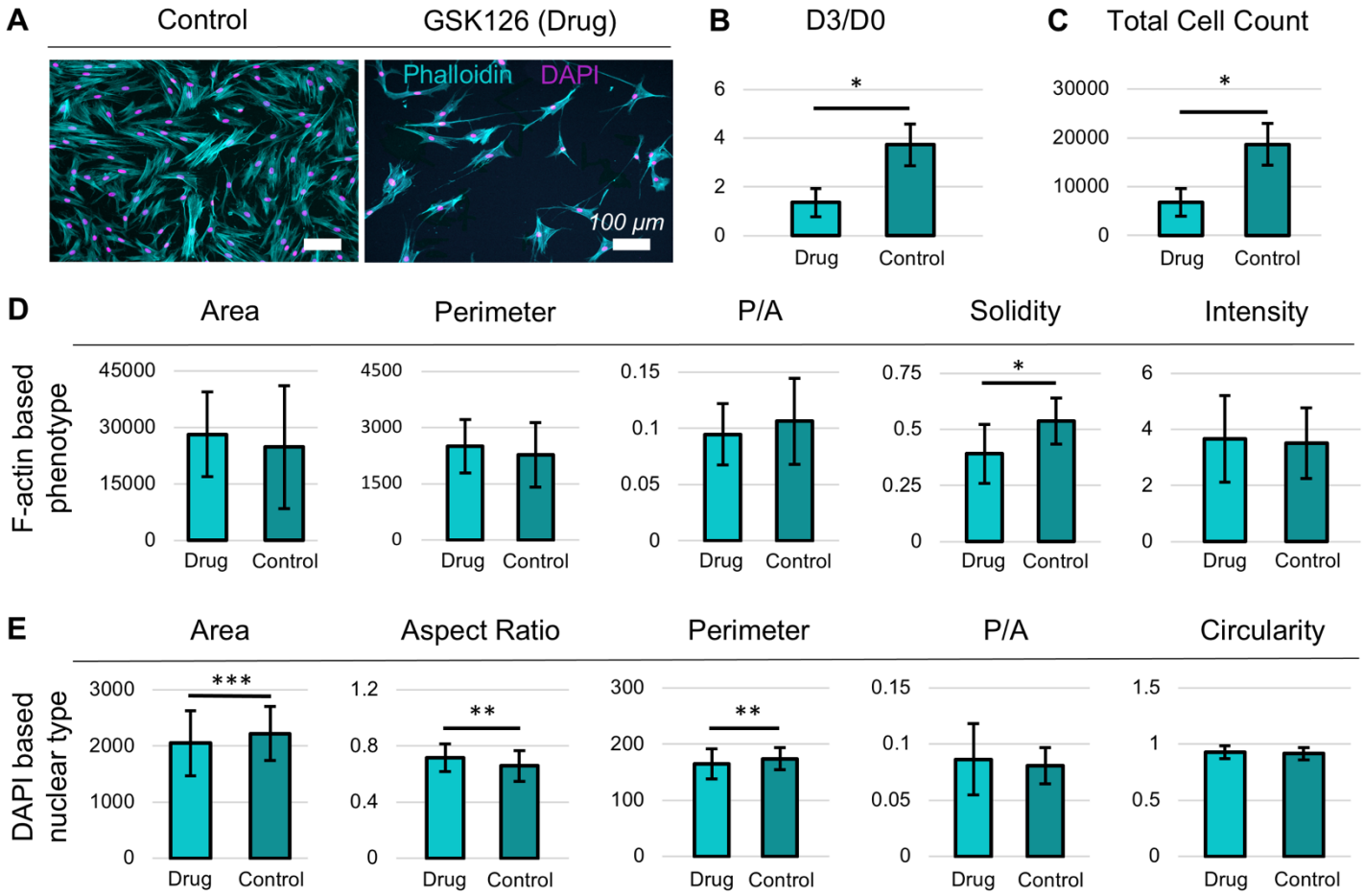

Figure 1. Effect of 20 µM GSK126 treatment on the proliferation and phenotype of human bone marrow derived primary MSC (hBM-MSC). (A) Representative images of Passage 4 MSC with phalloidin stained F-actin and DAPI stained nucleus on Day 3 after seeding. **(B)** Ratio of number of cells on Day 3 over Day 0. **(C)** Total number of cells on Day 3. **(D)** Different geometric shape parameters based upon cell phenotype. **(E)** Different geometric shape parameters based upon nuclear phenotype. Data based upon >4 technical replicates (>2000 cells per replicate) per group. *p <0.0001, **p <0.001, ***p <0.05.

leading to chromatin condensation. Considering the crucial role of chromatin remodeling in the mitotic chromatin condensation process, the observed decline in cell proliferation is unsurprising.

H3K27Me3 level is affected, but ARID1A and H3K4Me3 levels are not affected by the GSK126 treatment

GSK126, through its inhibition of EZH2, exerts an impact on chromatin remodeling and H3K27 methylation. Consequently, it is anticipated that this influence may extend to various epigenetic modifications, including levels of ARID1A, H3K27Me3, and H3K4Me3. To explore this possibility, confocal microscopy was employed to visualize key epigenetic modifiers, as illustrated in Figure 2.

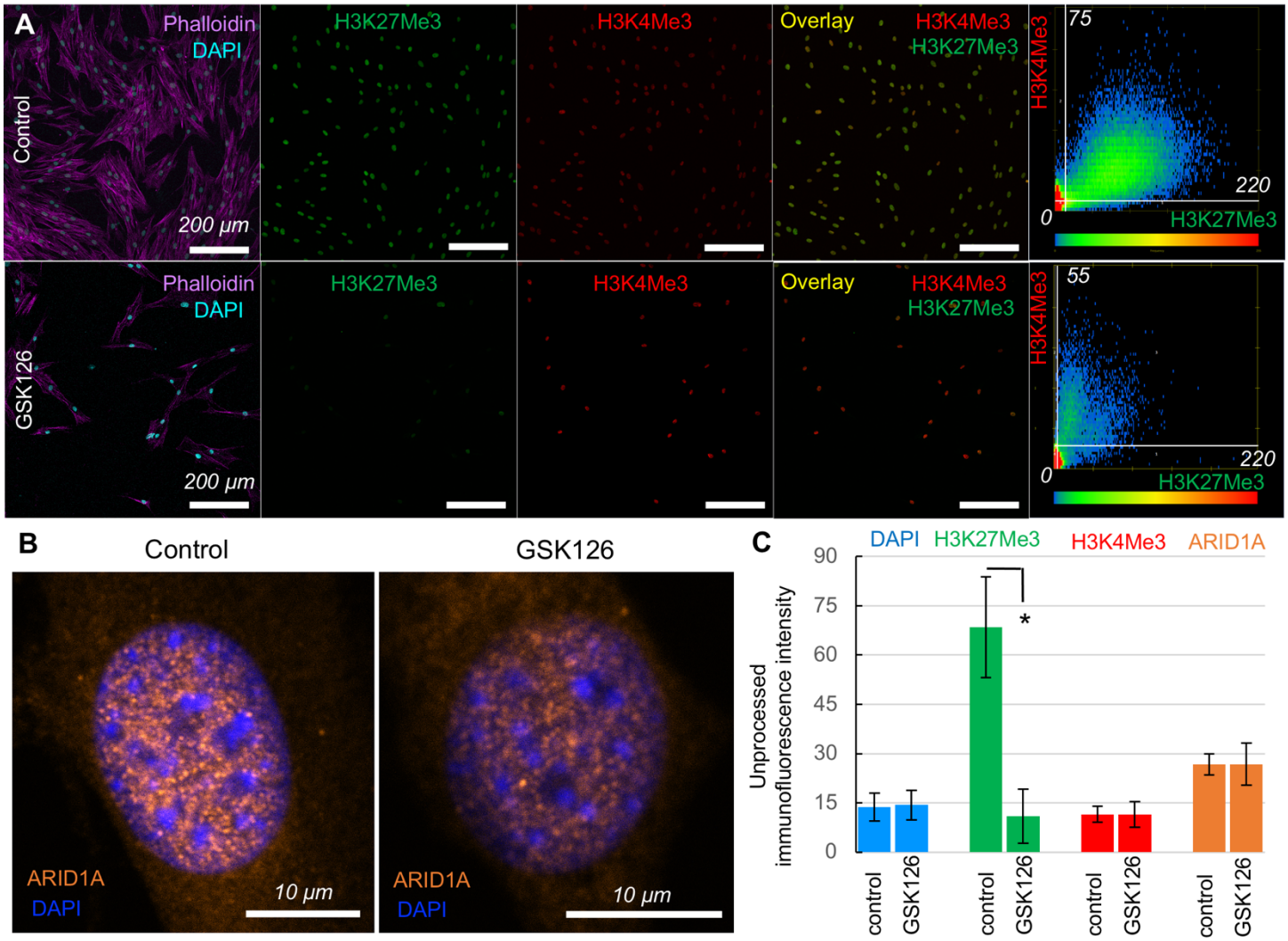

Figure 2. Effect of 20 µM GSK126 treatment on several epigenetic modifiers in hBM-MSC. (A) For both control and GSK126 treated groups, gene repression specific modifier H3K27Me3 and gene activation specific modifier H3K4Me3 are shown in unprocessed representative images to demonstrate their relative intensity levels. The scatterplot at the right panel shows the colocalization of H3K27Me3 and H3K4Me3 in the representative images. **(B)** High resolution confocal images of ARID1A and DAPI stained nuclei. **(C)** Unprocessed image Intensity based quantification of the intensity of epigenetic modifiers. Data based upon >4 technical replicates (>200 cells per replicate) per group. *p <0.001.

H3K4Me3, a specific epigenetic modifier associated with active gene regions, exhibited consistent intensity under GSK126 treatment. In contrast, H3K27Me3, linked to repressed genes, displayed a nearly sixfold

reduction in levels. Furthermore, colocalization analysis using Manders' Overlap Coefficient indicated a decrease in the simultaneous occurrence of H3K4Me3 and H3K27Me3 after a 3-day GSK126 treatment. Considering H3K27Me3's nature as a facultative repressive marker, signifying 'partially more open' chromatin in H3K27Me3 regions, GSK126 potentially induces alterations in euchromatin (open) and heterochromatin (closed) content within the nucleus.

Surprisingly, despite the known impact of EZH2 inhibition on ARID1A dynamics, the intensity level of ARID1A did not decrease with GSK126 treatment. Higher resolution confocal microscopy images revealed that GSK126 did not affect the intranuclear localization of ARID1A. Notably, ARID1A predominantly localized in euchromatin regions, evident in Figure 2B by the zones excluded by heavily DAPI-stained areas and areas excluded by DAPI-unstained regions, potentially populated by the nucleolus. This pattern remained consistent in both the control and GSK126-treated groups.

Hydrogen peroxide causes nuclear compaction which is inhibited by GSK126 treatment

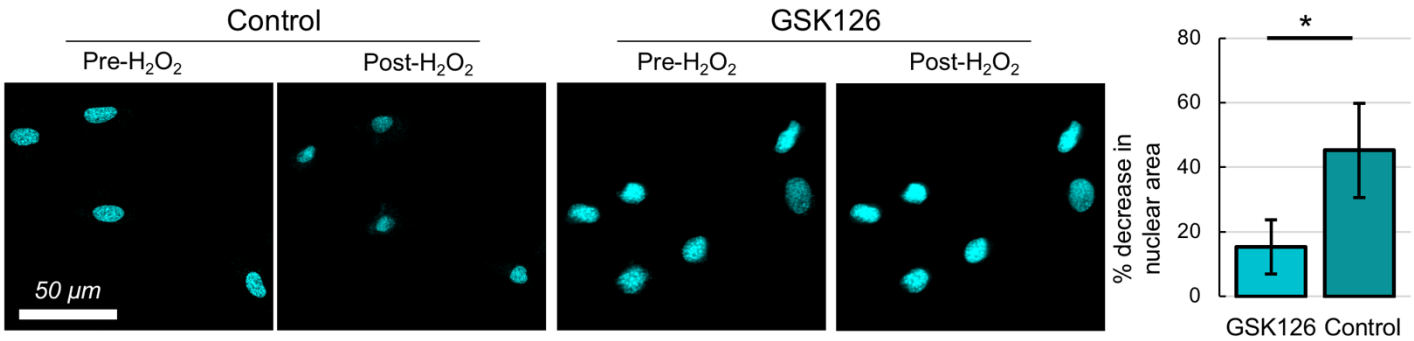

Figure 3. H_2O_2 (500 µM) driven nuclear shrinkage in hBM-MSC. Representative Images of Nucblue stained nuclei in live cells. Post-H_2O_2 corresponds to 75 min timepoint. Data based upon > 20 cells per group. *p <0.01.

Hyperoxia, characterized by elevated levels of reactive oxygen species beyond physiological norms, is recognized for its detrimental effects on cellular integrity. In this study, we sought to examine the impact of hydrogen peroxide exposure on cell nuclei and chromatin through live microscopy of individual cell nuclei stained with NucBlue, a live cell specific formulation of Hoechst. As depicted in Figure 3, nuclei in the control group exhibited shrinkage following exposure to 500 µM H_2O_2 treatment, whereas nuclei in the GSK126 pre-treated group maintained a relatively constant size, as quantified in the accompanying bar graph. The observed condensation in both cases persisted for approximately 75 to 80 minutes, after which nuclear size stabilized. This data highlights the phenomenon of chromatin condensation in response to H_2O_2 exposure, underscoring the essential role of chromatin remodeling in this process.

Chromatin remodeling is zone specific inside the nucleus

Utilizing high-resolution time-lapse imaging of individual nuclei stained with NucBlue during exposure to H_2O_2, active chromatin remodeling was observed, as depicted in Figure 4A. Notably, this remodeling was significantly halted by pre-treatment with GSK126. Chromatin Remodeling Index (CRI) maps illustrated spatial heterogeneity and temporal variability in the remodeling process. To discern the chromatin zone within the

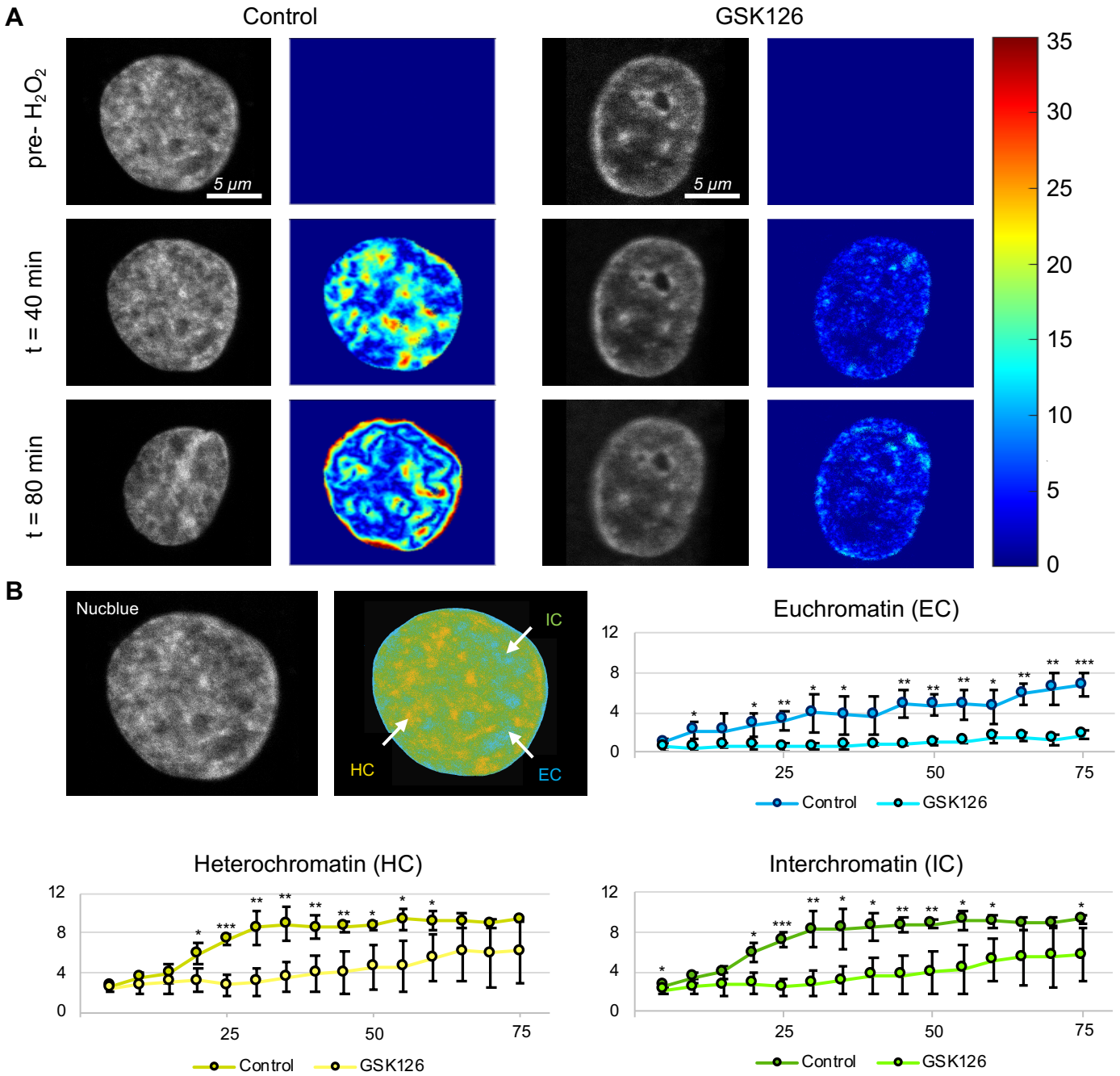

Figure 4. Chromatin remodeling in hBM-MSC under the exposure of 500 µM H_2O_2 (A) Time lapse image sequence at a few timepoints for representative nuclei without or with GSK126 treatment. Chromatin Remodeling Index map (displacement in pixels) is shown as colormap. 1 pixel = 21 nm. **(B)** Heterochromatin (HC), Euchromatin (EC) and Interchromatin (IC) domains shown for a representative nucleus. In the plots, X axis represent time (in minutes) and Y axis represents CRI in the specific domain. Data based on at least 5 nuclei per group. * $p < 0.05$ ** $p < 0.01$, *** $p < 0.001$.

nucleus undergoing the most pronounced remodeling, the intranuclear space was partitioned into three regions: euchromatin (open region), heterochromatin (closed region), and interchromatin (interface of heterochromatin and euchromatin).

Time-lapse average CRI values for each zone, as shown in Figure 4B, revealed that the euchromatin domain experienced the most substantial chromatin remodeling, particularly when compared to the GSK126 treated group. Additionally, chromatin remodeling in euchromatin persisted for an extended duration in comparison to the flatter time-lapse curves observed in the heterochromatin and interchromatin regions. This data suggests that GSK126 impedes the nanoscale chromatin remodeling process during H_2O_2 exposure.

H3K9Me3 level is differentially affected by GSK126 and hydrogen peroxide treatment

H3K9Me3 serves as an epigenetic modifier linked to constitutive heterochromatin, indicating its association with repressed regions that are not easily amenable to alteration. Upon visualizing and quantifying the intensity level of H3K9Me3, GSK126 demonstrated no significant impact on this particular epigenetic modifier, as illustrated in Figure 5.

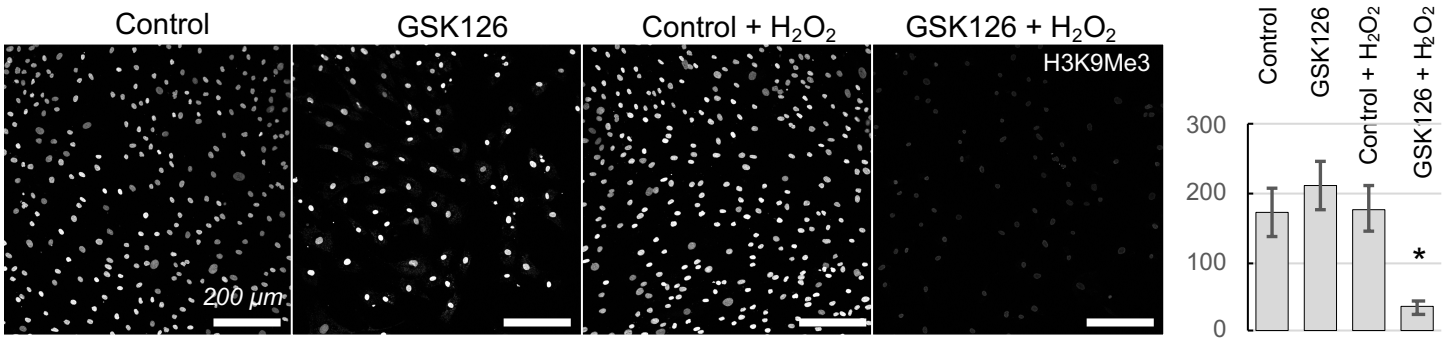

Figure 5. Effect of GSK126 and H_2O_2 treatment on the gene repression specific modifier H3K9Me3 in hBM-MSC. Representative unprocessed image of a field of view from each group. Data in the bar graph is based upon > 4 technical replicates (>200 cells per replicate) per group. *p <0.001.

Despite H_2O_2 induced nuclear condensation and chromatin remodeling observed (as stated in previous sections), the H3K9Me3 intensity level remained unchanged in the control group 24 hours post-treatment with H_2O_2. However, in the GSK126-treated group, where chromatin remodeling was impeded, a significantly lower amount of H3K9Me3 was observed 24 hours post-treatment with H_2O_2, suggesting a comprehensive alteration in epigenetic programming within the nucleus. It is noteworthy that in this experiment, H_2O_2 treatment persisted for 90 minutes, followed by complete removal of H_2O_2 and replenishment with fresh MSC medium. Similarly, the GSK126-treated group received fresh MSC medium containing GSK126.

GSK126 pre-treatment changes the DNA damage profile post H_2O_2 treatment

Reactive Oxygen Species are known to induce DNA damage, particularly through double-strand breaks (DSBs). Cells employ various strategies for DSB repair, with an increase in γ-H2AX (phosphorylated form of H2AX) levels and foci serving as markers of this repair response. Following 24 hours of H_2O_2 treatment, the overall intensity level of γ-H2AX exhibited a nearly 25% decrease due to GSK126 pre-treatment, as depicted in Figure 6A.

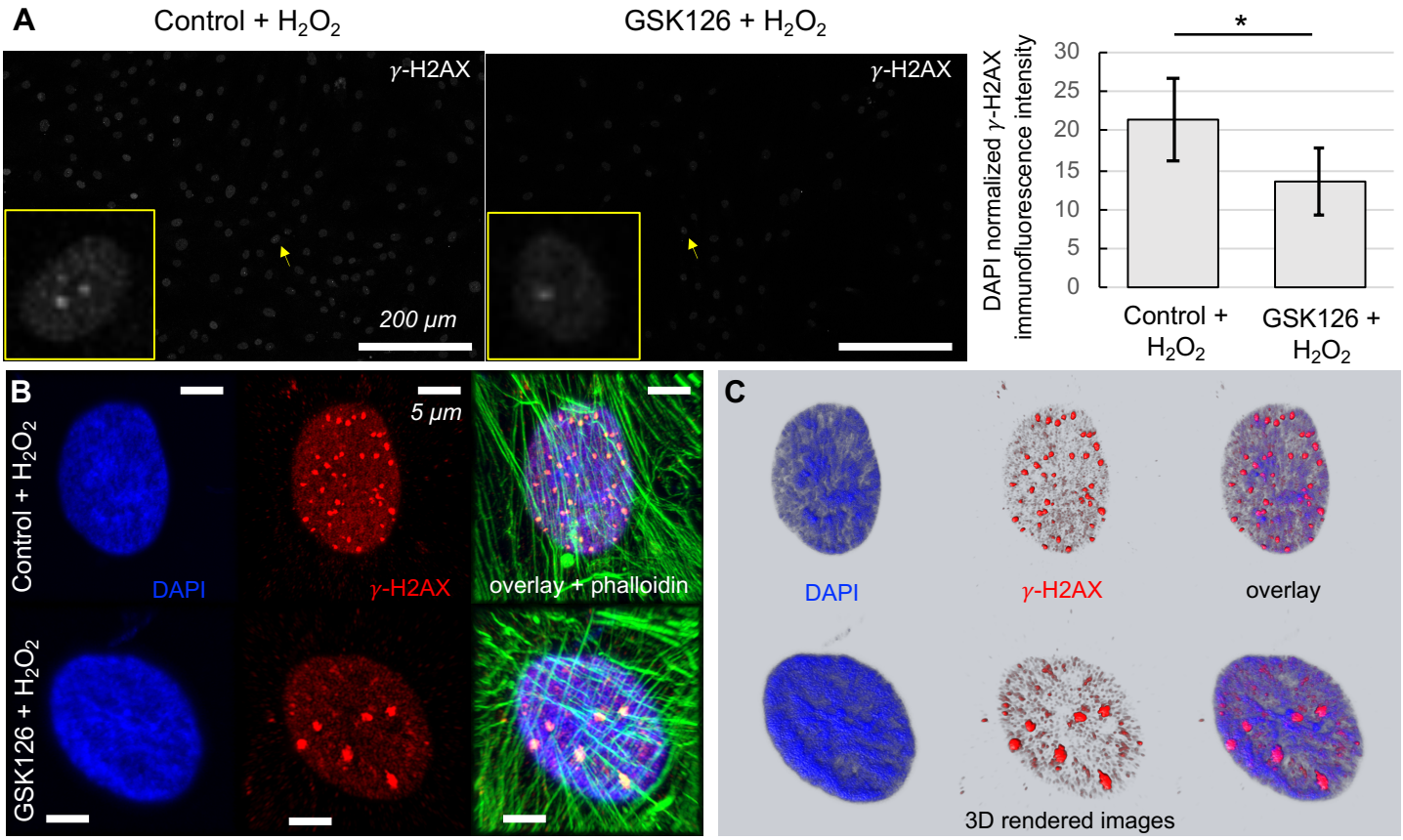

Figure 6. DNA damage in hBM-MSC on the exposure of H_2O_2. (A) Representative field of view of nuclei with the DNA damage marker γ-H2AX. Zoomed in view of a nucleus in each case is shown in the inset for the nucleus marked with an arrow. Dots represent the DNA damage foci. Bar diagram graph is based upon >4 technical replicates (>200 cells per replicate) per group. *p <0.01. **(B)** Super-resolution images of representative nucleus with multiple stains. **(C)** 3D rendering of the super-resolution images based upon z stacks showing the larger foci and smaller nanoscale foci.

While the distribution of the number of γ-H2AX foci appeared highly heterogeneous across all fields of view, the elevated intensity of γ-H2AX immunofluorescence correlated with a greater number of γ-H2AX foci. Super-resolution images of individual nuclei provided additional insights into the formation of γ-H2AX foci. As illustrated in Figure 6B, a representative case from the control group exhibited numerous visible γ-H2AX foci, whereas the nucleus from the GSK126-treated group displayed fewer foci, albeit larger in size. Further analysis through three-dimensional rendering of z-stack images (step size is 145 m) revealed that the majority of foci were

predominantly located in euchromatin zones, which are lightly stained with DAPI, as shown in Figure 6C. Additionally, many nano-sized globules of γ-H2AX foci were visible in both groups.

Cell viability post H_2O_2 exposure is not affected by the GSK126 pre-treatment

Subsequently, we explored the impact of GSK126 and H_2O_2 on cell viability (Figure 7). Treatment with 20 μM GSK126 did not adversely affect cell viability, suggesting the absence of toxic effects at this specified concentration. Exposure to 500 μM H_2O_2 for 90 minutes did not lead to a significant decrease in cell viability after 24 hours post H_2O_2 treatment. Likewise, pre-treatment with GSK126 did not exert any notable influence on cell viability, even following exposure to H_2O_2.

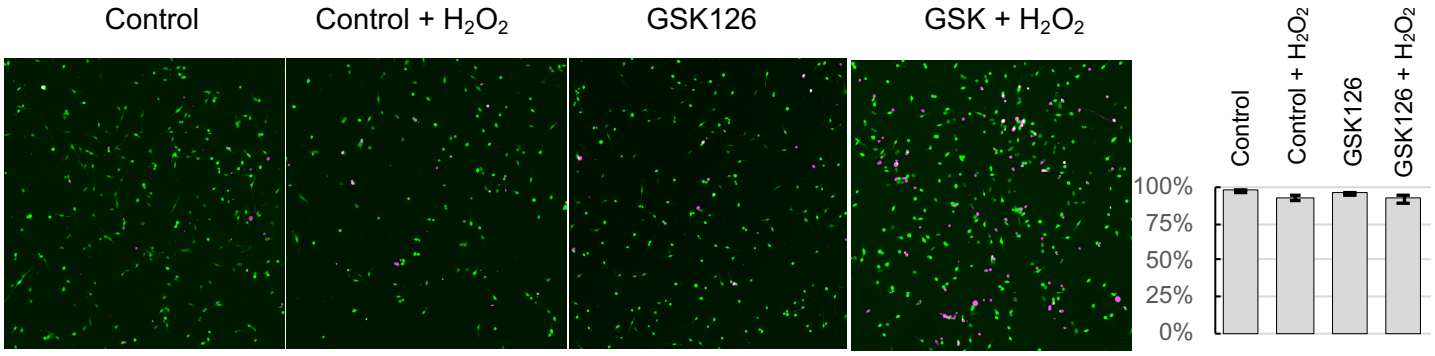

Figure 7. Viability of hBM-MSC on the exposure of H_2O_2. Representative images of the field of view from each group. Green represent all cells and pink represent dead cells. Bar graphs are based upon >4 technical replicates (>1000 cells per replicate) per group.

DISCUSSION

Overall, this work creates a technical framework to visualize and quantify the chromatin remodeling in real time. Chromatin remodeling and its functional significance is a budding research niche, and this work accomplishes to visualize such events using a specific cell type in a specific application. However, the technique can be applied to many applications in other cell types where real time visualization of chromatin remodeling can reveal new fundamental discoveries. A limitation of this technique is the use of NucBlue (a live imaging formulation of Hoechst) which is easily photobleached even at a very low laser power and it is not the optimal dye to image intranuclear architecture. Endogenous probes such as fluorescent H2B coding gene can be integrated to the chromatin for long-term imaging with a lower risk of photobleaching. With that modality of imaging, more ambitious questions can be answered such as how the chromatin compaction happens in 3D because using those probes, it is possible to capture the full 3D volumetric map of the nucleus. In this work, the third dimension was

very small. Therefore, the 2D representation of the CRI mapping is valid but 3D imaging with multiple images in the z stack will provide us with more insight into the CRI map.

ARID1A was identified as a possible key mediator of chromatin remodeling in this work. Although this is intriguing, we only used a single drug at a certain concentration. The drug we used (GSK126) indirectly blocks the ARID1A through inhibition of EZH2, although this is one of the most commonly used drugs for ARID1A inhibition (38). More direct blocking of ARID1A can be obtained through RNA interference strategy. It is not clear if ARID1A actually maintains the structural integrity of the chromatin or if it is actively engaged in the chromatin remodeling. Blocking multiple molecules in the SWI/SNF CRC might answer those questions. Interfacial phenomenon at the heterochromatin-euchromatin boundary is an emerging area of study. Observation of persistent and higher euchromatin remodeling is intriguing but it is not clear if this phenomenon is biophysical or biochemical, and what is the functional meaning of such remodeling in the euchromatin region. Further studies are required to discover any interesting mechanism that might be underlying such observation.

We observed several epigenetic modifications associated with the GSK126 treatment. The decrease in H3K27Me3 is not surprising given that it is facultative heterochromatin. Similarly, H3K9Me3 level was not affected by the GSK126 and this can be explained by the fact that the H3K9Me3 makes the constitutive heterochromatin which is difficult to amend. The drastic decrease in H3K9Me3 post hydrogen peroxide treatment is intriguing and needs further investigation. It is possible that the observed lack of chromatin remodeling and chromatin compaction in the GSK126 treated group upon hyperoxia forces the chromatin to stay open by a compensatory mechanism that may employ the decreasing of H3K9Me3. Of course, this will have consequences on the MSC functionality which can be revealed by several assays such as RNA seq and ChIP-seq.

DNA damage foci formation was revealed by the super-resolution microscopy. Interestingly, the GSK126 treatment showed modest decrease in the γ-H2AX formation after the oxidative stress was applied. It is not clear if this is detrimental or beneficial for cells because cell viability did not change in the GSK126 group after the application of hyperoxia. The fact that DNA damage foci was larger in GSK126 inhibited group can be explained as follows. It is possible that without GSK126, the chromatin compacts and many DNA damage lesions form which stay apart from each other due to the heterochromatin barrier created by the chromatin compaction and

remodeling. When the chromatin is more open, as in the case of GSK126 group, the damage lesions coalesce to create larger foci. Phase separation in chromatin has been reported recently and this phenomenon might be in line with several other studies (39).

Author contributions

S.G. conceived of the project. L.M., N.K. and S.G. conducted experiments. L.M., N.K., S.K. and S.G. contributed to data analysis. L.M. and S.G. wrote the manuscript with input from all authors. S.G. secured resources and funding for this study.

Acknowledgements

We acknowledge Abigail Fennell, Zack Aboellail, Jack Forman and Lillian Garfinkel for their contribution in imaging and data analysis.

Disclosure statement

No potential conflict of interest was reported by the authors.

Declaration of funding

The authors acknowledge the funding from the National Science Foundation (CAREER award, 2236710), which partially supported this work.

REFERENCES

1. Cooke, M.S., M.D. Evand, M. Dizdaroglu, and J. Lunec. 2003. Oxidative DNA damage: Mechanisms, mutation and disease. *FASEB Journal*. 17.
2. Liguori, I., and G. Russo. 2018. Oxidative stress, aging, and diseases. *Clinical Intervetions in Aging*. 13:757–772.
3. Mittal, M., M.R. Siddiqui, K. Tran, S.P. Reddy, and A.B. Malik. 2014. Reactive oxygen species in inflammation and tissue injury. *Antioxidants and Redox Signaling*. 20:1126–1167.
4. Zhou, X., Y. Hong, H. Zhang, and X. Li. 2020. Mesenchymal stem cell senescence and rejuvenation : Current status and challenges. *Frontiers in Cell and Developmental Biology*. 8:1–13.
5. Tower, J. 2012. Stress and stem cells. *Wiley Interdiscip Rev Dev Biol*. 1:1–18.
6. Vitale, I., G. Manic, R. De Maria, G. Kroemer, and L. Galluzzi. 2017. DNA damage in stem cells. *Molecular Cell*. 66:306–319.
7. Chen, F., Y. Liu, N. Wong, and J. Xiao. 2017. Oxidative stress in stem cell aging. *Cell Transplantation*. 26:1483–1495.
8. Nava, M.M., Y.A. Miroshnikova, L.C. Biggs, C.M. Niessen, K.N. Dahl, S.A. Wickstro, B. Hoffmann, R. Merkel, C.M. Niessen, K.N. Dahl, and S.A. Wickstrom. 2020. Heterochromatin driven nuclear softening protects the genome against mechanical stress-induced damage. *Cell*. 181:800–817.
9. Santos, Á., A.W. Cook, R.E. Gough, M. Schilling, A. Olszok, I. Brown, L. Wang, J. Aaron, M.L. Martin-fernandez, F. Rehfeldt, and C.P. Toseland. 2020. DNA damage reorganisation alters nuclear mechanics through chromatin. *bioRxiv*.
10. Miroshnikova, Y.A., I. Cohen, E. Ezhkova, and S.A. Wickstrom. 2019. Epigenetic gene regulation,

chromatin structure, and force-induced chromatin remodelling in epidermal development and homeostasis. *Current Opinion in Genetics & Development*. 55:46–51.
11. Miroshnikova, Y.A., M.M. Nava, and S.A. Wickstrom. 2017. Emerging roles of mechanical forces in chromatin regulation. *Journal of Cell Science*. 130.
12. Venit, T., S.R. Mahmood, and M. Endara-coll. 2020. Nuclear actin and myosin in chromatin regulation and maintenance of genome integrity. *International Review of Cell and Molecular Biology*. 6:1–42.
13. Spees, J.L., R.H. Lee, and C.A. Gregory. 2016. Mechanisms of mesenchymal stem/stromal cell function. *Stem Cell Research and Therapy*. 7.
14. Raheja, L.F., D.C. Genetos, A. Wong, and C.E. Yellowley. 2011. Hypoxic regulation of mesenchymal stem cell migration: The role of RhoA and HIF-1α. *Cell Biology International*. 35.
15. Toupadakis, C.A., J.L. Granick, M. Sagy, A. Wong, E. Ghassemi, D.J. Chung, D.L. Borjesson, and C.E. Yellowley. 2013. Mobilization of endogenous stem cell populations enhances fracture healing in a murine femoral fracture model. *Cytotherapy*. 15.
16. Wilson, S.S., A. Wong, C.A. Toupadakis, and C.E. Yellowley. 2015. Expression of angiopoietin-like protein 4 at the fracture site: Regulation by hypoxia and osteoblastic differentiation. *Journal of Orthopaedic Research*. 33.
17. Nguyen, P.D., and P.D. Currie. 2018. In vivo imaging: Shining a light on stem cells in the living animal. *Development*. 145.
18. Pacini, S., and M. Petrini. 2017. In search of in vivo MSC. *Frontiers in Cell and Developmental Biology*. 5.
19. Antebi, B., L.A. Rodriguez, K.P. Walker, A.M. Asher, R.M. Kamucheka, L. Alvarado, A. Mohammadipoor, and L.C. Cancio. 2018. Short-term physiological hypoxia potentiates the therapeutic function of mesenchymal stem cells. *Stem Cell Research and Therapy*. 9:265.
20. Anderson, D.E., B.D. Markway, D. Bond, H.E. McCarthy, and B. Johnstone. 2016. Responses to altered oxygen tension are distinct between human stem cells of high and low chondrogenic capacity. *Stem Cell Research and Therapy*. 7.
21. Elabd, C., T.E. Ichim, K. Miller, A. Anneling, V. Grinstein, V. Vargas, and F.J. Silva. 2018. Comparing atmospheric and hypoxic cultured mesenchymal stem cell transcriptome: Implication for stem cell therapies targeting intervertebral discs. *Journal of Translational Medicine*. 16.
22. Kwon, S.Y., S.Y. Chun, Y.S. Ha, D.H. Kim, J. Kim, P.H. Song, H.T. Kim, E.S. Yoo, B.S. Kim, and T.G. Kwon. 2017. Hypoxia enhances cell properties of human mesenchymal stem cells. *Tissue Engineering and Regenerative Medicine*. 14.
23. Luo, Z., F. Wu, E. Xue, L. Huang, P. Yan, X. Pan, and Y. Zhou. 2019. Hypoxia preconditioning promotes bone marrow mesenchymal stem cells survival by inducing HIF-1α in injured neuronal cells derived exosomes culture system. *Cell Death and Disease*. 10.
24. Ma, T., W.L. Grayson, M. Frohlich, and G. Vunjak-Novakovic. 2009. Hypoxia and stem cell-based engineering in mesenchymal tissues. *American Institute of Chemical Engineering*. 25.
25. Müller, J., K. Benz, M. Ahlers, C. Gaissmaier, and J. Mollenhauer. 2011. Hypoxic conditions during expansion culture prime human mesenchymal stromal precursor cells for chondrogenic differentiation in three-dimensional cultures. *Cell Transplantation*. 20.
26. Shaik, S., D. Hayes, J. Gimble, and R. Devireddy. 2017. Inducing heat shock proteins enhances the stemness of frozen-thawed adipose tissue-derived stem cells. *Stem Cells and Development*. 26.
27. Pattappa, G., B. Johnstone, J. Zellner, D. Docheva, and P. Angele. 2019. The importance of physioxia in mesenchymal stem cell chondrogenesis and the mechanisms controlling its response. *International Journal of Molecular Sciences*. 20.
28. Costantini, D. 2019. Understanding diversity in oxidative status and oxidative stress: The opportunities and challenges ahead. *The Journal of Experimental Biology*. 222.
29. Salmon, A.B., A. Richardson, and V.I. Pérez. 2010. Update on the oxidative stress theory of aging: Does oxidative stress play a role in aging or healthy aging? *Free Radical Biology and Medicine*. 48.
30. Denu, R.A., and P. Hematti. 2016. Effects of oxidative stress on mesenchymal stem cell biology. *Oxidative Medicine and Cellular Longevity*. 10.
31. Vono, R., E. Jover Garcia, G. Spinetti, and P. Madeddu. 2018. Oxidative stress in mesenchymal stem cell

senescence: Regulation by coding and noncoding RNAs. *Antioxidants and Redox Signaling*. 29.
32. Zeng, W., J. Xiao, G. Zheng, F. Xing, G.L. Tipoe, X. Wang, C. He, Z. Chen, and Y. Liu. 2015. Antioxidant treatment enhances human mesenchymal stem cell anti-stress ability and therapeutic efficacy in an acute liver failure model. *Scientific reports*. 5.
33. Kumar, S., R. Verma, N. Tyagi, G. Gangenahalli, and Y.K. Verma. 2022. Therapeutics effect of mesenchymal stromal cells in reactive oxygen species-induced damages. *Human Cell*. 35.
34. Bitler, B.G., K.M. Aird, A. Garipov, H. Li, M. Amatangelo, A. V Kossenkov, D.C. Schultz, Q. Liu, I. Shih, J.R. Conejo-garcia, D.W. Speicher, and R. Zhang. 2015. Synthetic lethality by targeting EZH2 methyltransferase activity in ARID1A -mutated cancers. *Nature Medicine*. 21.
35. Kaonis, S., J. Forman, Z. Aboellail, and S. Ghosh. 2023. High-throughput multiparametric quantification of mechanics driven heterogeneity in mesenchymal stromal ell population. *Advanced Biology*.
36. Bay, B.K. 1995. Texture correlation: a method for the measurement of detailed strain distributions within trabecular bone. *Journal of Orthopaedic Research*. 13.
37. Ghosh, S., V.C. Cuevas, B. Seelbinder, and C.P. Neu. 2021. Image based elastography of heterochromatin and euchromatin domains in the deforming cell nucleus. *Small*. 17.
38. Niedermaier, B., A. Sak, E. Zernickel, S. Xu, M. Groneberg, and M. Stuschke. 2019. Targeting ARID1A-mutant colorectal cancer: depletion of ARID1B increases radiosensitivity and modulates DNA damage response. *Scientific Reports*. 9.
39. Hansen, J.C., K. Maeshima, and M.J. Hendzel. 2021. The solid and liquid states of chromatin. *Epigenetics & Chromatin*. 14.